ACS Catalysis
pubs.acs.org/acscatalysis
Research Article

Understanding the Roles of Hydroxide in CO_2 Electroreduction on a Cu Electrode for Achieving Variable Selectivity

Mingxu Sun, Aleksandar Staykov, and Miho Yamauchi*

Cite This: *ACS Catal.* 2022, 12, 14856−14863
Read Online

ACCESS | Metrics & More | Article Recommendations | Supporting Information

ABSTRACT: Hydroxide-derived copper (OH/Cu) electrodes exhibit excellent performance for the electrocatalytic CO_2 reduction reaction (CO_2RR). However, the role of hydroxide (OH) in CO_2RR remains controversial; therefore, the origin of the selectivity enhancement emerging on OH/Cu has not been fully understood. In the present work, we quantitatively evaluated surface OH by electroadsorption and established a direct correlation between the OH amount and selectivity for the production of CH_4 and C_{2+} on OH/Cu with the help of computational investigations concerning work functions of the surface. Based on these findings, we demonstrated variable selectivity using OH/Cu electrodes having a controlled OH amount; three OH/Cu electrodes realized their distinct selectivity such as Faradic efficiency (FE) for the production of CH_4 (CH_4 FE) of 78%, C_{2+} FE of 71%, and the ratio of C_{2+}-to-CH_4 >355. The proposed simple strategy for selectivity control would contribute to further quantity synthesis of value-added chemicals using CO_2RR.

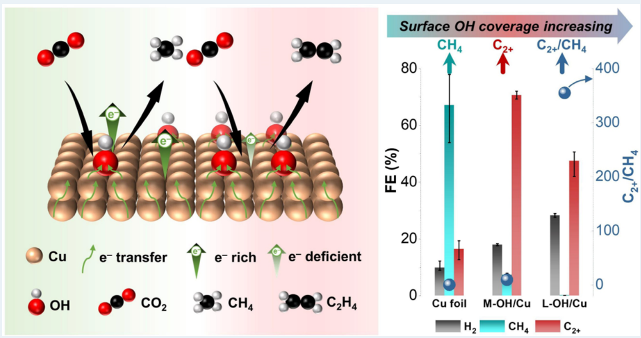

KEYWORDS: *CO_2 reduction reaction, hydroxide, work function, electroadsorption, variable selectivity*

INTRODUCTION

The selective CO_2RR into high value-added chemicals is increasingly in demand because it can mitigate the ever-increasing CO_2 emissions while achieving the utilization of reduction products such as CH_4, C_2H_4, and C_2H_5OH.[1−6] As one of the most representative Cu-based catalysts, hydroxide Cu or hydroxide-derived Cu (OH/Cu) has drawn the most attention because of its high selectivity toward C_{2+} chemicals.[7−10] Surprisingly, the origin of such excellent performance on OH/Cu has not been comprehensively understood yet. The controversy has revolved around the presence of oxidized Cu phases during CO_2RR.[9,11] With the development of in situ technologies, many researchers found that the oxidized Cu was completely reduced to metallic Cu after electrolysis.[8,12] Nevertheless, the main reason that enhances selectivity has been recently attributed to roughness factors,[7,13] crystal size,[8] and Cu facets,[10] although OH formation is the most obvious characteristic that distinguishes OH/Cu from the other Cu electrode materials. A key point is whether OH is present on OH/Cu during CO_2RR. As the reduction reaction involves a decrease in OH coverage on the Cu surface, OH remaining on the surface is hardly determined by ex situ measurements. In situ/operando spectroscopic characterizations are a strong tool to elucidate the state of the working surface, whereas they cannot distinguish the origins of objectives; whether they are derived from the electrode surface or electrolyte solutions. For instance, in situ surface-enhanced Raman spectroscopy (SERS) experiments have been conducted under conditions with a relatively high current density and nonbuffering electrolytes where the OH concentration at the electrode−electrolyte interface is sharply increased,[14,15] and therefore it is difficult to identify whether the OH originates from the electrode or aqueous solution.[16]

One less discussed, but arguably more important question is whether OH really affects selectivity or is merely a spectator in CO_2RR. Iijima et al. suggested that OH binding to the Cu surface can induce interactions of proximal CO to promote activity for the formation of C_{2+} chemicals.[17] Kimura et al. conducted CO_2RR on Cu catalysts by applying a pulsed potential and found that OH layers formed on the Cu surface sustain CO_2RR activity and enhance the selectivity for CH_4 production.[18] The center of the debate has been what product selectivity can be improved by OH formation, not the intrinsic nature of the electrode surface. Thus, we evaluated the influence of the OH coverage on the work function (WF) of

Received: July 26, 2022
Revised: October 14, 2022

https://doi.org/10.1021/acscatal.2c03650
ACS Catal. 2022, 12, 14856−14863

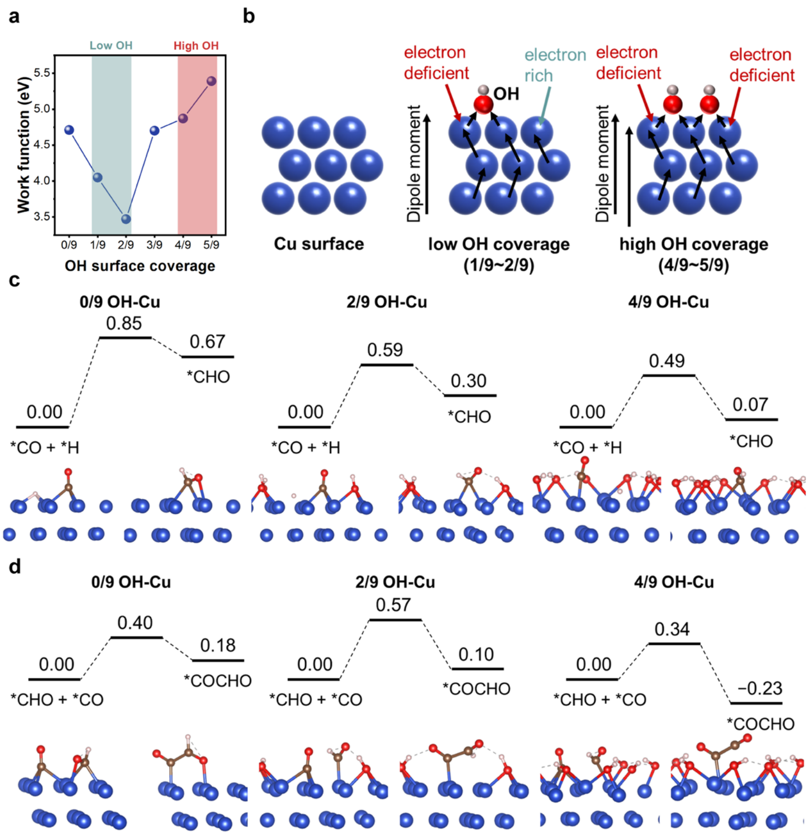

Figure 1. DFT calculation results. (a) Work functions calculated on the Cu surface with OH coverage in the range of 0/9−5/9. (b) Influence of OH on the surface electronic properties. Reaction energetics for (c) *CO hydrogenation to *CHO and (d) dimerization of *CHO and *CO to *COCHO on Cu surfaces with OH coverage of 0/9, 2/9, and 4/9. The geometries of reactants and products are displayed, including the top two Cu layers. All energy values are described in eV. Cu, O, C, and H are denoted in blue, red, brown, and white, respectively.

Cu surfaces, which is an indicator for the reducibility on the surface and is used for thermal hydrogenation such as ammonia synthesis.[19,20] The reaction energetics and the formation of the main intermediates such as *CHO and *COCHO, which are deeply related to the selectivity for the production of CH_4 and C_{2+} chemicals, respectively, were also explored. Our computational investigation results suggested that the product selectivity on the Cu surface can be steered by the amount of OH. Inspired by the density functional theory (DFT) results, we demonstrated a highly sensitive and quantitative characterization of an electrode surface to establish a direct correlation between the OH amount and the selectivity of CH_4 and C_{2+}, which is a missing piece in the CO_2RR research. Based on these findings, we prepared three Cu electrodes with different amounts of OH and demonstrated variable selectivity on the OH/Cu electrodes for the first time.

RESULTS AND DISCUSSION

We estimated the WFs of Cu surfaces with the following OH coverages: 0/9, 1/9, 2/9, 3/9, 4/9, and 5/9, where the ratio denotes the number of OH per surface Cu atom, using DFT as described in the Experimental Methods. For reference, the experimentally estimated WF value of the pristine (111) Cu surface was 4.70 eV. A nonlinear dependence of WF with OH surface functionalization is shown in Figure 1a. Compared with the pristine Cu surface, the low (1/9−2/9) and high (above 4/9) OH surface coverage regimes were characterized by smaller and larger WF values, respectively. Milliken population analysis indicated that the surface is moderately negatively charged at a low OH surface coverage (below 3/9), whereas all surface Cu atoms are positively charged at high OH surface coverage (above 4/9), as shown in Figure S1 and Table S1. As a result, at low OH coverage, the electronegative OH induces a dipole moment that increases the electron density on the surface Cu atoms and thereby enhances the electron transfer toward the outside of the surface. At a high OH coverage, the dipole moment of the Cu surface increases and the electron density is localized on the OH instead of on the surface Cu atoms owing to the dense OH termination (Figure 1b). In other words, the Cu surface with lower OH is more reductive than the pristine Cu surface and the Cu surface with higher OH. Such changes in the reducibility on the surface may affect the selectivity in CO_2RR.

On the basis of previous studies, hydrogenation of *CO to *CHO and the dimerization of *CHO and *CO for the formation of *COCHO have been recognized as controlling processes in the production of CH_4 and C_{2+}, respectively, in the CO_2RR;[21−23] therefore, we calculated the reaction energetics on the Cu surfaces with OH coverages of 0/9, 2/9, and 4/9 (Figure 1c,d). We found that the systematic increase in the OH coverage from 0/9 to 4/9 reduces the activation barrier of *CO hydrogenation from 0.85 to 0.49 eV and stabilizes the *CHO on the Cu surface (Figure 1c). The 2/9 OH coverage shows the highest activation barrier (0.57 eV) for the *COCHO formation, whereas the 4/9 OH coverage affords the lowest activation barrier (0.34 eV) and exothermic *COCHO formation (Figure 1d). These results indicate that low OH coverage is more favorable for CH_4

https://doi.org/10.1021/acscatal.2c03650
ACS Catal. 2022, 12, 14856−14863

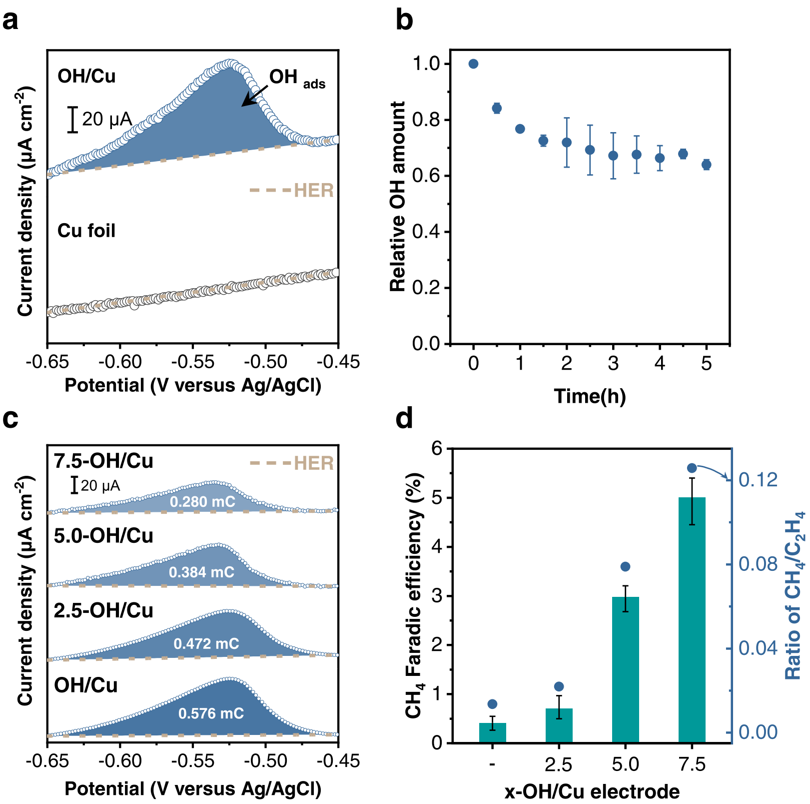

Figure 2. Characterization of surface OH and CO_2RR performance on OH/Cu electrodes. (a) LSV curves measured on a Cu foil and OH/Cu at 10 $mV\cdot s^{-1}$ in Ar-saturated 0.1 M $KHCO_3$. A yellow dashed curve represents a fitted line for the HER current, which is regarded as a baseline. (b) Relative OH amounts formed during CO_2RR at −1.0 V versus RHE. The OH amount was quantified by the charge for the OH electroadsorption and a relative OH amount was calculated by the ratio of areas for the OH electroadsorption per 0.5 h and that at 0 h. (c) LSV measurements for OH/Cu, 2.5-OH/Cu, 5.0-OH/Cu, and 7.5-OH/Cu at 10 $mV\cdot s^{-1}$ in Ar-saturated 0.1 M $KHCO_3$. (d) CH_4 FE and the ratio of CH_4/C_2H_4 on OH/Cu, 2.5-OH/Cu, 5.0-OH/Cu, and 7.5-OH/Cu at −50 mA cm^{-2} in CO_2-saturated 0.1 M $KHCO_3$.

formation, whereas high OH coverage possibly induces the production of C_{2+}. These DFT results clearly suggest that the OH coverage significantly modifies the reactivity on the Cu surface. Thus, we try to explore the method to correlate the OH amount on the electrode surface with the CO_2RR selectivity.

In general, spectroscopic probes for observing a surface are placed at a distance from the sample and collect signals generated in the whole sample space. Then, we focused on an electrochemical probe that only detects signals through contact points on a surface to limit signal sources. From the early study on the electrochemical oxidation of metallic Cu, we learned that the adsorption process of OH on an electrode surface occurs in alkaline conditions at a potential before the onset of Cu_2O formation,[24−26] which involves sequential transitions from lattice Cu atoms (Cu) to adsorbed Cu atoms (Cu*), eventually leading to the Cu*-hydrous ($Cu^*(OH)_{ads}$).[25]

To clearly observe the OH adsorption, we compared the cyclic voltammetry (CV) curves measured on a Cu foil in KOH and $KHCO_3$ electrolyte solutions. To avoid side reactions, argon was continued to be purged during the electrochemical measurements.[27] An obvious oxidation current peak at −0.62 V versus Ag/AgCl was obtained with KOH but not with $KHCO_3$ (Figure S2). The peak observed in the KOH solution is possibly attributed to electrochemical OH adsorption where OH mainly comes from the alkaline electrolyte (KOH).[28] Then, we sought to measure the surface OH on OH/Cu using the OH electroadsorption technique with a neutral electrolyte ($KHCO_3$). An OH/Cu electrode was prepared by the electroreduction (−0.6 V versus RHE) of a Cu foil covered with $Cu(OH)_2$, which was synthesized by the electrooxidation of a Cu foil in the KOH solution at 22 °C. The CV showed an OH electroadsorption peak on OH/Cu before the onset of Cu_2O formation in the $KHCO_3$ solution (Figure S3). An expansion of a linear sweep voltammetry (LSV) profile of the OH/Cu revealed that an OH adsorption peak appeared in the potential range from −0.65 to −0.45 V versus Ag/AgCl but not on a Cu foil (Figure 2a). This result indicated that the origin of OH is relevant to the characteristics of the electrode. To confirm the presence of OH during CO_2RR, we applied −1.0 V versus RHE as a near-reaction potential and estimated the OH amount on the electrode surface. The amount of OH was quantified by the number of charges corresponding to an OH electroadsorption peak (Figure S4 and Table S2) and the relative OH amount was calculated from the ratio of the electroadsorption area per 0.5 h to that at 0 h, as shown in Figure 2b. The error bars for the relative OH amounts are probably ascribed to the accompanying CO_2RR, which effects the OH electrosorption process.[27] These results suggested that OH is not considerably consumed during CO_2RR. The prereduction condition for the preparation of OH/Cu electrodes might affect the OH amount. Thus, we prepared three electrodes through the further prereduction of the as-prepared OH/Cu at different potentials (−2.5, −5.0, and −7.5 V versus Ag/AgCl) for 0.5 hours, namely, 2.5-OH/Cu, 5.0-OH/Cu, and 7.5-OH/Cu, respectively. Although the

https://doi.org/10.1021/acscatal.2c03650
ACS Catal. 2022, 12, 14856−14863

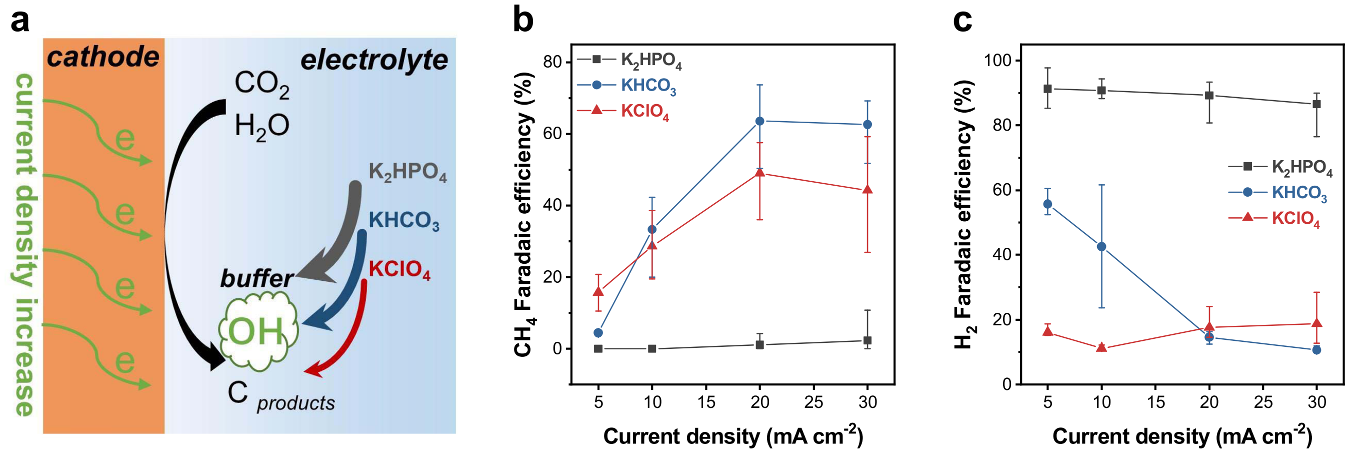

Figure 3. CO_2RR performance in different buffer solutions. (a) Schematic image of the OH environment produced in K_2HPO_4, $KHCO_3$, and $KClO_4$ during CO_2RR. Faradic efficiency for (b) CH_4 and (c) H_2 in K_2HPO_4, $KHCO_3$, and $KClO_4$.

peak area for the OH electroadsorption measured on the three electrodes exhibited a downward trend as a more negative potential was applied in the prereduction, the surface OH still remained on the electrode surface (Figure 2c).

Next, the CO_2RR performance was evaluated by applying the constant current of −50 mA cm^{-2}, and the product distribution is given in Figure S5. Figure 2d provides CH_4 FE and the ratio of CH_4-to-C_2H_4 observed on each OH/Cu electrode. As the OH amount decreased, both CH_4 FE and the ratio of CH_4-to-C_2H_4 increased, suggesting that a low OH coverage is feasible for the CH_4 formation as predicted by DFT calculations (Figure 1c,d). However, C_2H_4 FE did not keep declining with a decrease in the OH amount (Figure S5d). Considering that H_2 FE decreased with a decrease in the OH amount, FE for carbon products is possibly related to the suppression of HER (Figure S5b). We examined first whether the difference in HER was caused by the effects of the roughness factors on CO_2 diffusion. The roughness factors were estimated from the electrochemical surface area (ECSA) and were not found to be correlated to HER and CO_2RR performances as shown in Figure S6. Our DFT calculations suggested that the HER may also be affected by the OH amount, and then we estimated the reaction energy for H_2 dissociation and H_2 evolution on Cu surfaces with 2/9 and 4/9 OH coverages (Figure S7 and Tables S3 and S4). The H_2 evolution on the surface with 2/9 OH coverage has an activation barrier of 0.63 eV, whereas that on the surface with 4/9 OH coverage exhibits a barrierless or downhill of −0.57 eV. Therefore, the amount of surface OH not only controls the product selectivity but also balances the CO_2 conversion and HER.

Although this study provides evidence that the selectivity for the CH_4 production is enhanced with a decrease in the OH amount, the selective production of CH_4 using an OH/Cu electrode has never been reported, which motivates us to achieve high CH_4 FE. As seen in Figure 2d, the CH_4 FE gradually increased as the OH amount decreased and exhibited a further upward trend, suggesting that the OH amount formed in this experiment was not optimal for CH_4 production. Then, we apply a Cu foil as an electrode, which is covered by a few OH generated during CO_2RR, to minimize the amount of the surface OH. Considering that each e$^-$ transfer produces 1 equivalent of OH,[16] the amount of OH on the electrode surface largely depends on the current density. Moreover, the OH released during CO_2RR can be neutralized by shifting the equilibrium of reactions such as, $OH^- + HPO_4^{2-} \rightarrow H_2O + PO_4^{3-}$, and $OH^- + HCO_3^- \rightarrow H_2O + CO_3^{2-}$, which are developed in the electrolytes including HPO_4^{2-} and HCO_3^-.[29,30] To obtain an ideal amount of OH produced by CO_2RR, we systematically examined the CO_2RR performance on a Cu foil by employing three electrolytes with different buffering abilities for OH (Figure 3a). The buffering abilities were in the order of $K_2HPO_4 > KHCO_3 > KClO_4$, and the OH concentration around the electrode surface will be mitigated to different extents in the order of $K_2HPO_4 < KHCO_3 < KClO_4$. The CO_2RR performance on a Cu foil was evaluated in the CO_2-saturated 0.1 M K_2PO_4, $KHCO_3$, or $KClO_4$ electrolyte at a constant current density from −5 to −30 mA cm^{-2} (Figure S8). As the current density increased, applications of $KHCO_3$ and $KClO_4$ significantly improved the CH_4 FE (Figure 3b), whereas HER preferentially proceeded with K_2HPO_4 (Figure 3c). This demonstrates the positive effect of the OH formed during CO_2RR on improving CH_4 selectivity. The buffering ability of $KHCO_3$ provides the most favorable environment for the selective production of CH_4 (Figure 3b). It should be noted that the inclusion of $KClO_4$ exhibited a relatively high C_2H_4 FE as shown in Figure S8. Furthermore, CO_2RR in K_2HPO_4 always resulted in H_2 FE as high as 90%, even though the current density reached 30 mA cm^{-2} (Figure 3c), which indicated that OH played a crucial role in the selectivity control in CO_2RR. This result is consistent with that of the effect of O on CO_2RR.[31] Interestingly, when the current density increased to more than 20 mA cm^{-2}, the H_2 FE with $KClO_4$ unexpectedly increased, which was larger than that observed with $KHCO_3$ (Figure 3c). This phenomenon once again provides evidence for this view that relatively high OH amounts on the electrode surface promote the HER as shown in Figures S5 and S7.

These findings led us to synthesize three electrodes characterized by significantly different OH amounts: small (**Cu foil**), moderate (**M-OH/Cu**), and large amounts of OH (**L-OH/Cu**). The processes for the preparation of **M-OH/Cu** and **L-OH/Cu** are illustrated in Figure 4a. A surface $Cu(OH)_2$ layer was formed on a Cu foil through electrooxidation at 0 °C (i-$Cu(OH)_2$/Cu), and **M-OH/Cu** was obtained by a harsh reduction process via temperature-programmed H_2 reduction. **L-OH/Cu** was prepared by the electroreduction of $Cu(OH)_2$/Cu, which was synthesized via the electrooxidation of a Cu foil

https://doi.org/10.1021/acscatal.2c03650
ACS Catal. 2022, 12, 14856−14863

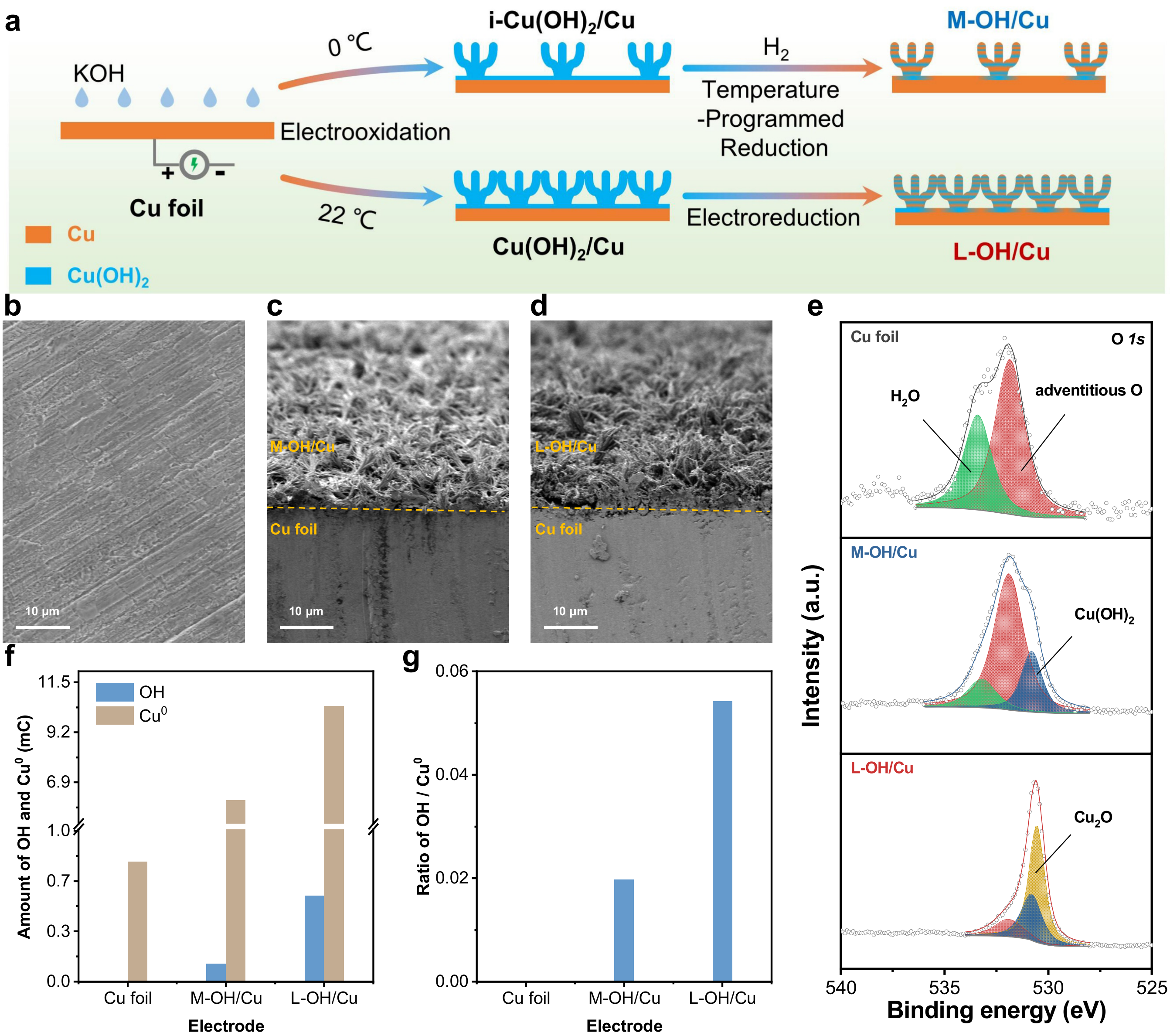

Figure 4. Synthetic routine and structural characterizations. (a) Schematic synthetic procedure for **M-OH/Cu** and **L-OH/Cu**. (b) SEM image of **Cu foil**. Cross-sectional SEM images of (c) **M-OH/Cu** and (d) **L-OH/Cu**. (e) XPS spectrum of O 1s for **Cu foil**, **M-OH/Cu**, and **L-OH/Cu**. Amount (f) and ratio (g) of OH and Cu^0 (OH quantified by the charge of OH electroadsorption, Cu^0 quantified by the charge of Cu_2O formation) for **Cu foil**, **M-OH/Cu**, and **L-OH/Cu**.

at 22 °C. X-ray diffraction (XRD) and Raman spectroscopy indicated that the surface of i-$Cu(OH)_2$/Cu and $Cu(OH)_2$/Cu was composed only of $Cu(OH)_2$ (Figure S9). Scanning electron microscopy (SEM) suggested that the pristine **Cu foil** has a relatively flat surface (Figure 4b), whereas needle-like nanostructures are formed on the surface of **M-OH/Cu** and **L-OH/Cu**, which was confirmed by a cross-sectional SEM measurement (Figure 4c,d). High-resolution transmission electron microscopy (HRTEM) indicated that **L-OH/Cu** is a Cu electrode containing $Cu(OH)_2$. Observed lattice fringes with interplanar spacings of 0.209 and 0.226 nm correspond well to the (111) lattice plane of Cu and the (130) lattice plane of $Cu(OH)_2$, respectively (Figure S10).[32] Further characterization of the electrode composition was performed using X-ray photoelectron spectroscopy (XPS). Cu $2p_{3/2}$ peaks observed at 932.6 eV correspond to the Cu^0 state of **Cu foil**, and peaks at 932.8 eV in **M-OH/Cu** and at 932.65 eV in **L-OH/Cu**, with a very small shift from the Cu^0 state, suggest that the surfaces of these samples are somewhat oxidized (Figure S11). It is difficult to distinguish the oxidation states between Cu^0 and Cu^1 using the Cu $2p_{3/2}$ signals since the binding energies of the two species differ by only 0.1 eV; the binding energy of Cu^0 is 932.6 eV and that of Cu^1 is 932.5 eV. The Cu LMM spectrum showed a peak at 918.6 eV, which corresponded to metallic Cu, whereas the peaks at 916.2−916.4 eV assignable to Cu_2O or $Cu(OH)_2$ were too close to be separated (Figure S12).[17,33] XPS observation of the O 1s enabled us to distinguish Cu_2O from $Cu(OH)_2$ (Figures 4e and S13). $Cu(OH)_2$ (530.8 eV) existed on the surface of **M-OH/Cu**, whereas $Cu(OH)_2$ (530.8 eV) and Cu_2O (530.5 eV) coexisted on the surface of **L-OH/Cu** (Figure 4e). The other O 1s peaks located at 533.4 and 531.9 eV are assigned to water and adventitious oxygen.[34−36] Since the electroreduction process of **L-OH/Cu** was conducted in an aqueous solution,

https://doi.org/10.1021/acscatal.2c03650
ACS Catal. 2022, 12, 14856−14863

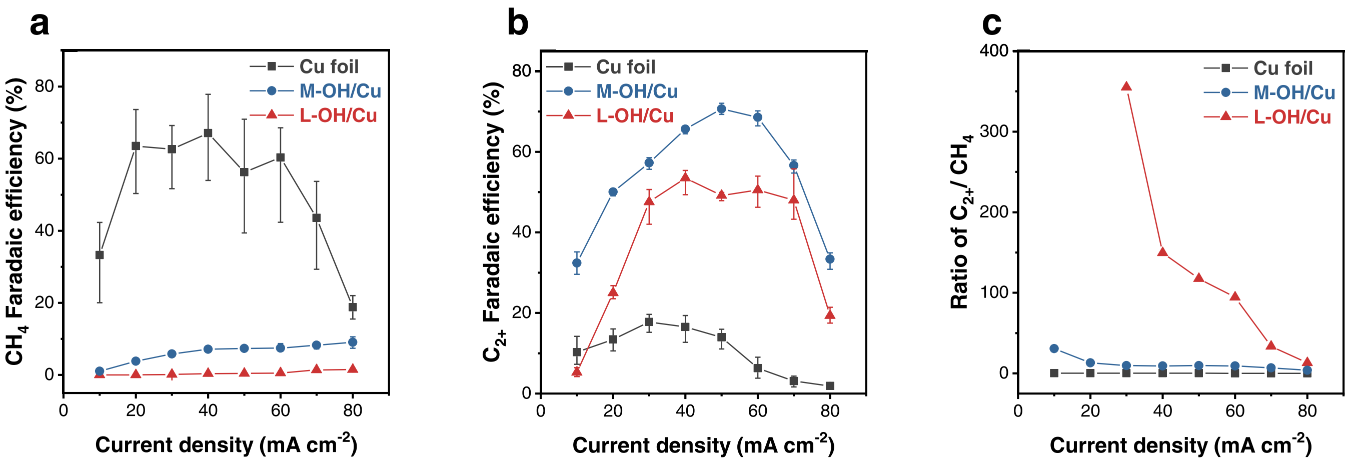

Figure 5. CO_2RR performance. FE of (a) CH_4 and (b) C_{2+} and (c) ratio of C_{2+}-to-CH_4 for **Cu foil**, **M-OH/Cu**, and **L-OH/Cu**.

Cu_2O possibly originates from ambient oxidation. Then, we conducted Raman spectroscopy as shown in Figure S14. The Raman peaks observed at 220 and 630 cm^{-1}, which were attributed to the Raman-allowed modes of $2\Gamma_{12-}$ and $\Gamma_{12-} + \Gamma_{25+}$ of the Cu_2O, were observed only on **L-OH/Cu**, whereas these peaks disappeared at an applied potential of −0.6 V versus RHE (Figure S14).[37] We quantified the OH amount on each Cu electrode surface based on OH electroadsorption and the Cu^0 amount was calculated from the peak area for the Cu oxidation to form Cu_2O (Figure 4f). These values were normalized with the charge contributing to the corresponding peak (Figures S15 and S16 and Table S5). The amount of OH and the OH-to-Cu^0 ratio on **L-OH/Cu** were 4.7 times and 2.7 times, respectively, larger than those on **M-OH/Cu** (Figure 4f,g).

The CO_2RR performance was evaluated by a constant current density mode at current densities from −10 to −80 mA cm^{-2} using a gastight H-type glass cell. Figure S17 shows the current-dependent FE for all products on **Cu foil**, **M-OH/Cu**, and **L-OH/Cu**, and differences in applied potential possibly come from different ECSA values (Figure S18). As we expected, with the increase in the applied current density, the **Cu foil** exhibited a significant increase in CH_4 selectivity. An average CH_4 FE of 67% and a maximum CH_4 FE of 78% with a partial current density of 41 mA cm^{-2} were achieved (Figures 5a and S20). Furthermore, the H_2 FE was suppressed to be less than 9% (Figure S19). The large error bar for CH_4 FE on **Cu foil**, as shown in Figure 5a, possibly came from the buffering of electrolyte, which competes with the OH generation during CO_2RR.[38,39] **M-OH/Cu** characterized by the moderate OH amount showed a C_{2+} FE of 71% and a partial current density of 41 mA cm^{-2} (Figures 5b and S20), where the main C_{2+} product was C_2H_4 with an FE of 46% and a partial current density of 28 mA cm^{-2} (Figures S19 and S20). Based on the proposed mechanism for the HER suppression, **L-OH/Cu** having a large OH amount exhibited a lower C_{2+} FE (54%) than **M-OH/Cu** (71%), but the ratio of C_{2+}-to-CH_4 is as high as >355 (Figure 5c). According to SEM and XPS characterization results, the **M-OH/Cu** and **L-OH/Cu** after CO_2RR still had OH in them and kept needle-like nanostructures (Figures S21−S24).

■ CONCLUSIONS

In this work, we investigated the origin of the enhanced selectivity on OH/Cu electrodes and found that the surface OH greatly drives selectivity in CO_2RR. DFT calculations revealed that the surface OH significantly affects the WFs and the reduction ability of Cu surfaces. This is the first insight into the relevance of WFs on the electrode to its CO_2RR activity. Combined with OH electroadsorption characterization and CO_2RR performance, we elucidated a direct relationship between the OH amount and selectivity for the production of CH_4 and C_{2+} for the first time. Finally, we demonstrated variable selectivity on Cu electrodes by controlling the OH amounts; CH_4 FE of 78% on **Cu foil**, C_{2+} FE of 71% on **M-OH/Cu**, and the ratio of C_{2+}-to-CH_4 >355 on **L-OH/Cu**. This study provided new insights into the mechanism of CO_2RR on OH/Cu electrodes while offering a simple and effective way to achieve highly selective CO_2RR.

■ ASSOCIATED CONTENT

Supporting Information

The Supporting Information is available free of charge at https://pubs.acs.org/doi/10.1021/acscatal.2c03650.

Detailed computational and experimental methods and additional XRD, Raman, TEM, XPS, DFT data, and other electrochemical measurements (PDF)

■ AUTHOR INFORMATION

Corresponding Author

Miho Yamauchi − *Department of Chemistry, Graduate School of Science, Kyushu University, Fukuoka 819-0395, Japan; International Institute for Carbon-Neutral Energy Research (WPI-I²CNER), Research Center for Negative Emissions Technologies (K-Nets), and Institute for Materials Chemistry and Engineering (IMCE), Kyushu University, Fukuoka 819-0395, Japan; Advanced Institute for Materials Research (WPI-AIMR), Tohoku University, Sendai 980-8577, Japan;* orcid.org/0000-0003-4752-172X; Email: yamauchi@ms.ifoc.kyushu-u.ac.jp

Authors

Mingxu Sun − *Department of Chemistry, Graduate School of Science, Kyushu University, Fukuoka 819-0395, Japan*

Aleksandar Staykov − *International Institute for Carbon-Neutral Energy Research (WPI-I²CNER) and Research*

https://doi.org/10.1021/acscatal.2c03650
ACS Catal. 2022, 12, 14856−14863

Center for Negative Emissions Technologies (K-Nets), Kyushu University, Fukuoka 819-0395, Japan; orcid.org/0000-0003-2572-1317

Complete contact information is available at:
https://pubs.acs.org/10.1021/acscatal.2c03650

Notes

The authors declare no competing financial interest.

■ ACKNOWLEDGMENTS

The authors acknowledge funding from JST (JPMJFS2132), JSPS KAKENHI (JP18H05517 "Hydrogenomics" and 22K19088), and the Moonshot Research and Development Program (JPNP18016)

■ REFERENCES

(1) Bushuyev, O. S.; De Luna, P.; Dinh, C. T.; Tao, L.; Saur, G.; van de Lagemaat, J.; Kelley, S. O.; Sargent, E. H. What Should We Make with CO_2 and How Can We Make It? *Joule* **2018**, *2*, 825−832.

(2) Hori, Y.; Kikuchi, K.; Suzuki, S. Production of CO and CH_4 in Electrochemical Reduction of CO_2 at Metal Electrodes in Aqueous Hydrogencarbonate Solution. *Chem. Lett.* **1985**, *14*, 1695−1698.

(3) Hori, Y.; Wakebe, H.; Tsukamoto, T.; Koga, O. Electrocatalytic Process of CO Selectivity in Electrochemical Reduction of CO_2 at Metal Electrodes in Aqueous Media. *Electrochim. Acta* **1994**, *39*, 1833−1839.

(4) Ma, S.; Sadakiyo, M.; Heima, M.; Luo, R.; Haasch, R. T.; Gold, J. I.; Yamauchi, M.; Kenis, P. J. Electroreduction of Carbon Dioxide to Hydrocarbons Using Bimetallic Cu−Pd Catalysts with Different Mixing Patterns. *J. Am. Chem. Soc.* **2017**, *139*, 47−50.

(5) Anzai, A.; Liu, M.-H.; Ura, K.; Noguchi, T. G.; Yoshizawa, A.; Kato, K.; Sugiyama, T.; Yamauchi, M. Cu Modified TiO_2 Catalyst for Electrochemical Reduction of Carbon Dioxide to Methane. *Catalysts* **2022**, *12*, 478.

(6) Yamauchi, M. Inorganic Nanocatalysts for Hydrogenation Reactions Contributable to a Sustainable Material Supply. *Chem. Lett.* **2021**, *50*, 1901−1908.

(7) Ma, M.; Djanashvili, K.; Smith, W. A. Controllable Hydrocarbon Formation from the Electrochemical Reduction of CO_2 over Cu Nanowire Arrays. *Angew. Chem., Int. Ed.* **2016**, *55*, 6680−6684.

(8) Lei, Q.; Zhu, H.; Song, K.; Wei, N.; Liu, L.; Zhang, D.; Yin, J.; Dong, X.; Yao, K.; Wang, N.; Li, X.; Davaasuren, B.; Wang, J.; Han, Y. Investigating the Origin of Enhanced C_{2+} Selectivity in Oxide-/Hydroxide-Derived Copper Electrodes during CO_2 Electroreduction. *J. Am. Chem. Soc.* **2020**, *142*, 4213−4222.

(9) Lee, S. Y.; Jung, H.; Kim, N. K.; Oh, H. S.; Min, B. K.; Hwang, Y. J. Mixed Copper States in Anodized Cu Electrocatalyst for Stable and Selective Ethylene Production from CO_2 Reduction. *J. Am. Chem. Soc.* **2018**, *140*, 8681−8689.

(10) Zhong, D.; Zhao, Z. J.; Zhao, Q.; Cheng, D.; Liu, B.; Zhang, G.; Deng, W.; Dong, H.; Zhang, L.; Li, J.; Li, J.; Gong, J. Coupling of Cu(100) and (110) Facets Promotes Carbon Dioxide Conversion to Hydrocarbons and Alcohols. *Angew. Chem., Int. Ed.* **2021**, *60*, 4879−4885.

(11) Farmand, M.; Landers, A. T.; Lin, J. C.; Feaster, J. T.; Beeman, J. W.; Ye, Y.; Clark, E. L.; Higgins, D.; Yano, J.; Davis, R. C.; Mehta, A.; Jaramillo, T. F.; Hahn, C.; Drisdell, W. S. Electrochemical Flow Cell Enabling Operando Probing of Electrocatalyst Surfaces by X-ray Spectroscopy and Diffraction. *Phys. Chem. Chem. Phys.* **2019**, *21*, 5402−5408.

(12) Kim, T.; Kargar, A.; Luo, Y.; Mohammed, R.; Martinez-Loran, E.; Ganapathi, A.; Shah, P.; Fenning, D. P. Enhancing C_2−C_3 Production from CO_2 on Copper Electrocatalysts via a Potential-Dependent Mesostructure. *ACS Appl. Energy Mater.* **2018**, *1*, 1965−1972.

(13) Jiang, K.; Huang, Y.; Zeng, G.; Toma, F. M.; Goddard, W. A.; Bell, A. T. Effects of Surface Roughness on the Electrochemical Reduction of CO_2 over Cu. *ACS Energy Lett.* **2020**, *5*, 1206−1214.

(14) Chang, X.; Zhao, Y.; Xu, B. pH Dependence of Cu Surface Speciation in the Electrochemical CO Reduction Reaction. *ACS Catal.* **2020**, *10*, 13737−13747.

(15) Zhao, Y.; Chang, X.; Malkani, A. S.; Yang, X.; Thompson, L.; Jiao, F.; Xu, B. Speciation of Cu Surfaces During the Electrochemical CO Reduction Reaction. *J. Am. Chem. Soc.* **2020**, *142*, 9735−9743.

(16) Nitopi, S.; Bertheussen, E.; Scott, S. B.; Liu, X.; Engstfeld, A. K.; Horch, S.; Seger, B.; Stephens, I. E. L.; Chan, K.; Hahn, C.; Norskov, J. K.; Jaramillo, T. F.; Chorkendorff, I. Progress and Perspectives of Electrochemical CO_2 Reduction on Copper in Aqueous Electrolyte. *Chem. Rev.* **2019**, *119*, 7610−7672.

(17) Iijima, G.; Inomata, T.; Yamaguchi, H.; Ito, M.; Masuda, H. Role of a Hydroxide Layer on Cu Electrodes in Electrochemical CO_2 Reduction. *ACS Catal.* **2019**, *9*, 6305−6319.

(18) Kimura, K. W.; Casebolt, R.; Cimada DaSilva, J.; Kauffman, E.; Kim, J.; Dunbar, T. A.; Pollock, C. J.; Suntivich, J.; Hanrath, T. Selective Electrochemical CO_2 Reduction during Pulsed Potential Stems from Dynamic Interface. *ACS Catal.* **2020**, *10*, 8632−8639.

(19) Kitano, M.; Inoue, Y.; Ishikawa, H.; Yamagata, K.; Nakao, T.; Tada, T.; Matsuishi, S.; Yokoyama, T.; Hara, M.; Hosono, H. Essential Role of Hydride Ion in Ruthenium-based Ammonia Synthesis Catalysts. *Chem. Sci.* **2016**, *7*, 4036−4043.

(20) Ye, T. N.; Park, S. W.; Lu, Y.; Li, J.; Sasase, M.; Kitano, M.; Tada, T.; Hosono, H. Vacancy-enabled N_2 Activation for Ammonia Synthesis on an Ni-loaded Catalyst. *Nature* **2020**, *583*, 391−395.

(21) Cheng, T.; Xiao, H.; Goddard, W. A., 3rd Free-Energy Barriers and Reaction Mechanisms for the Electrochemical Reduction of CO on the Cu(100) Surface, Including Multiple Layers of Explicit Solvent at pH 0. *J. Phys. Chem. Lett.* **2015**, *6*, 4767−4773.

(22) Garza, A. J.; Bell, A. T.; Head-Gordon, M. Mechanism of CO2 Reduction at Copper Surfaces: Pathways to C_2 Products. *ACS Catal.* **2018**, *8*, 1490−1499.

(23) Liu, X.; Schlexer, P.; Xiao, J.; Ji, Y.; Wang, L.; Sandberg, R. B.; Tang, M.; Brown, K. S.; Peng, H.; Ringe, S.; Hahn, C.; Jaramillo, T. F.; Norskov, J. K.; Chan, K. pH Effects on the Electrochemical Reduction of $CO_{(2)}$ towards C_2 Products on Stepped Copper. *Nat. Commun.* **2019**, *10*, No. 32.

(24) Martins, M. E.; Arvia, A. J. Enhancement of Current Peak multiplicity Related to Cuprous Oxide Electroreduction and Transient Copper Activation in Alkaline Solution. *J. Electroanal. Chem.* **1984**, *165*, 135−145.

(25) Gennero De Chialvo, M. R.; Zerbino, J.; Marchiano, S.; Arvia, A. Correlation of Electrochemical and Ellipsometric Data in Relation to the Kinetics and Mechanism of Cu_2O Electroformation in Alkaline Solutions. *J. Appl. Electrochem.* **1986**, *16*, 517−526.

(26) Burke, L. D.; Ryan, T. The Participation of Interfacial Hydrous Oxide Species in Some Anodic Reactions at Copper Electrodes in Base. *J. Electrochem. Soc.* **1990**, *137*, 1358.

(27) Lee, S. H.; Lin, J. C.; Farmand, M.; Landers, A. T.; Feaster, J. T.; Aviles Acosta, J. E.; Beeman, J. W.; Ye, Y.; Yano, J.; Mehta, A.; Davis, R. C.; Jaramillo, T. F.; Hahn, C.; Drisdell, W. S. Oxidation State and Surface Reconstruction of Cu under CO_2 Reduction Conditions from In Situ X-ray Characterization. *J. Am. Chem. Soc.* **2021**, *143*, 588−592.

(28) Caballero-Briones, F.; Artés, J. M.; Díez-Pérez, I.; Gorostiza, P.; Sanz, F. Direct Observation of the Valence Band Edge by In Situ ECSTM-ECTS in p-type Cu_2O Layers Prepared by Copper Anodization. *J. Phys. Chem. C* **2009**, *113*, 1028−1036.

(29) Hori, Y.; Murata, A.; Takahashi, R.; Suzuki, S. J. o. t. C. S. Chemical Communications, Enhanced Formation of Ethylene and Alcohols at Ambient Temperature and Pressure in Electrochemical Reduction of Carbon Dioxide at a Copper Electrode. *J. Chem. Soc., Chem. Commun.* **1988**, *1*, 17−19.

(30) Hori, Y.; Murata, A.; Takahashi, R. Formation of Hydrocarbons in the Electrochemical Reduction of Carbon Dioxide at a Copper

Electrode in Aqueous Solution. *J. Chem. Soc., Faraday Trans. 1* **1989**, *85*, 2309−2326.
(31) Liu, G.; Lee, M.; Kwon, S.; Zeng, G.; Eichhorn, J.; Buckley, A. K.; Toste, F. D.; Goddard, W. A., 3rd; Toma, F. M. CO_2 Reduction on Pure Cu Produces Only H_2 After Subsurface O is Depleted: Theory and Experiment. *Proc. Natl. Acad. Sci. U.S.A.* **2021**, *118*, No. e2012649118.
(32) Du, G. H.; Van Tendeloo, G. $Cu(OH)_2$ Nanowires, CuO Nanowires and CuO Nanobelts. *Chem. Phys. Lett.* **2004**, *393*, 64−69.
(33) Platzman, I.; Brener, R.; Haick, H.; Tannenbaum, R. J. Oxidation of Polycrystalline Copper Thin Films at Ambient Conditions. *J. Phys. Chem. C* **2008**, *112*, 1101−1108.
(34) Poulston, S.; Parlett, P.; Stone, P.; Bowker, M. Surface Oxidation and Reduction of CuO and Cu_2O Studied Using XPS and XAES. *Surf. Interface Anal.* **1996**, *24*, 811−820.
(35) Wang, W. Z.; Wang, G.; Wang, X. S.; Zhan, Y.; Liu, Y.; Zheng, C. L. Synthesis and Characterization of Cu_2O Nanowires by a Novel Reduction Route. *Adv. Mater.* **2002**, *14*, 67−69.
(36) Eilert, A.; Cavalca, F.; Roberts, F. S.; Osterwalder, J.; Liu, C.; Favaro, M.; Crumlin, E. J.; Ogasawara, H.; Friebel, D.; Pettersson, L. G.; Nilsson, A. Subsurface Oxygen in Oxide-Derived Copper Electrocatalysts for Carbon Dioxide Reduction. *J Phys Chem Lett* **2017**, *8*, 285−290.
(37) Deng, Y.; Handoko, A. D.; Du, Y.; Xi, S.; Yeo, B. S. In Situ Raman Spectroscopy of Copper and Copper Oxide Surfaces during Electrochemical Oxygen Evolution Reaction: Identification of Cu^{III} Oxides as Catalytically Active Species. *ACS Catal.* **2016**, *6*, 2473−2481.
(38) Gupta, N.; Gattrell, M.; MacDougall, B. Calculation for the Cathode Surface Concentrations in the Electrochemical Reduction of CO_2 in $KHCO_3$ Solutions. *J. Appl. Electrochem.* **2006**, *36*, 161−172.
(39) Gattrell, M.; Gupta, N.; Co, A. A Review of the Aqueous Electrochemical Reduction of CO_2 to Hydrocarbons at Copper. *J. Electroanal. Chem.* **2006**, *594*, 1−19.

https://doi.org/10.1021/acscatal.2c03650
ACS Catal. 2022, 12, 14856−14863